
SAFE CONTROL WITH NEURAL NETWORK DYNAMIC MODELS

A PREPRINT

Tianhao Wei

Carnegie Mellon University
twei2@andrew.cmu.edu

Changliu Liu

Carnegie Mellon University
cliu6@andrew.cmu.edu

October 5, 2021

ABSTRACT

Safety is critical in autonomous robotic systems. A safe control law ensures forward invariance of a safe set (a subset in the state space). It has been extensively studied regarding how to derive a safe control law with a control-affine analytical dynamic model. However, in complex environments and tasks, it is challenging and time-consuming to obtain a principled analytical model of the system. In these situations, data-driven learning is extensively used and the learned models are encoded in neural networks. How to formally derive a safe control law with Neural Network Dynamic Models (NNDM) remains unclear due to the lack of computationally tractable methods to deal with these black-box functions. In fact, even finding the control that minimizes an objective for NNDM without any safety constraint is still challenging. In this work, we propose MIND-SIS (Mixed Integer for Neural network Dynamic model with Safety Index Synthesis), the first method to derive safe control laws for NNDM. The method includes two parts: 1) SIS: an algorithm for the offline synthesis of the safety index (also called as barrier function), which uses evolutionary methods and 2) MIND: an algorithm for online computation of the optimal and safe control signal, which solves a constrained optimization using a computationally efficient encoding of neural networks. It has been theoretically proved that MIND-SIS guarantees forward invariance and finite convergence. And it has been numerically validated that MIND-SIS achieves safe and optimal control of NNDM. From our experiments, the optimality gap is less than 10^{-8} , and the safety constraint violation is 0.

Keywords Safe control, neural network dynamics, model-based RL.

1 Introduction

Safety is a major concern of autonomous robotic systems, which can usually be posed as constraint satisfaction problems, such as collision avoidance for vehicles and speed limitation of robot arms. Robot safety depends on the correct functioning of all system components, such as accurate perception, safe motion planning, and safe control. Safe control, as the last defense of system safety, has been widely studied in the context of dynamical systems [1, 2]. A safe control law is a control law that ensures the forward invariance of a subset inside the safety constraint. That means, once the state entered that subset, it will never leave. If we have a control-affine analytical dynamic model of the system, there are many methods to derive the corresponding safe control laws [3–5]. However, constructing such an analytical dynamic model for complex systems can be difficult, time-consuming, and sometimes impossible [6]. Recent works adopt data-driven approaches to learn these dynamic models, and most of the learned models are encoded in neural networks.

Examples of these neural network dynamic models (NNDM) include virtual world models in video games or dynamic models of a complicated integrated robot, etc [7, 8]. Although NNDMs can greatly alleviate human efforts in modeling, they are less interpretable than analytical models. It is more challenging to derive control laws, especially safe control laws, for these NNDMs than for analytical models.

This paper focuses on safe tracking tasks with NNDMs, which is formulated as a constrained optimization that minimizes the state tracking error given the safety constraint and the NNDM constraint. Even without the safety constraint, the tracking control with NNDMs is already challenging. Existing control-theoretical methods usually use model in-

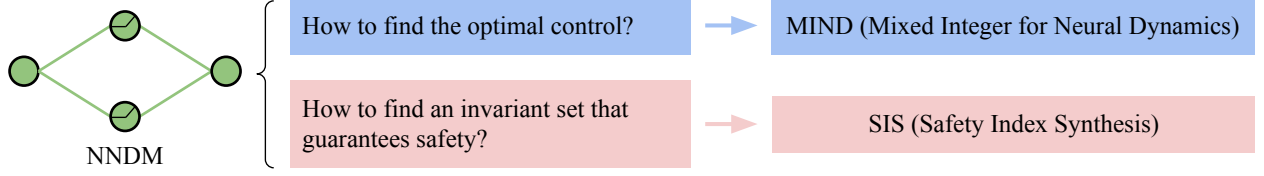


Figure 1: Overview of MIND-SIS.

verse [9] to compute the desired control inputs to track a state trajectory. Since NNDMs are complex and highly nonlinear, there is no computationally efficient method to compute its model inverse. A widely used method to control NNDMs in practice is the shooting method, which randomly generates many candidate controls and rolls out corresponding future states, then chooses the control leads to the closest state to the reference state. But the shooting method is both incomplete and sub-optimal. That means, it is not guaranteed to find a solution when the problem is feasible, and even if it finds a solution, the solution may not be the best one that optimizes the control objective. Moreover, the safety constraint adds another layer of difficulty to the problem. The robot should not only select an action that satisfies the safety constraint now but also ensure that its current action will not end up in any future state that no action is safe. This property is called *persistent feasibility*. To ensure persistent feasibility, we need to compute the control invariant set inside the original safety constraint and constrain the robot motion in this more restrictive control invariant set. For an analytical model, we can manually craft this control invariant set to meet the requirement [4]. But this becomes difficult for NNDM due to its poor interpretability.

In this work, we address these challenges by introducing an integrated method MIND-SIS to handle both the offline synthesis of the control invariant set and the online computation of the constrained optimization with NNDM constraints as shown in fig. 1. Inspired from neural network verification algorithms [10, 11], we use mixed integer programming (MIP) to encode the NNDMs in the constraint, which makes the constrained optimization much easier to solve. Most importantly, the MIP method is complete and guarantees optimality, *i.e.* it can always find the optimal control that minimizes the control objective under constraints. To synthesize the control invariant set, we first parameterize a safety index whose zero sub-level set should be the control invariant set and then use evolutionary algorithms to learn the parameters of the safety index. By substituting the original safety constraint with the new constraint from the learned safety index, the resulting control inputs from the constrained optimization will ensure forward invariance inside the safety constraint.

The remaining of the paper is organized as follows. Section 2 provides a formal description of the problem and introduces notations to be used. Section 3 introduces prior works on safe control, NNDM, and neural network verification, which inspires our method. Section 4 discusses the proposed method in detail. Section 5 shows experimental results that validate our method. And section 6 discusses possible future directions.

2 Formulation

Dynamic model Consider a discrete time dynamical system with m_x state and m_u controls.

$$\mathbf{x}_{k+1} = \mathbf{x}_k + \mathbf{f}(\mathbf{x}_k, \mathbf{u}_k)dt \quad (1)$$

where k is the time step, $\mathbf{x}_k \in X \subset \mathbb{R}^{m_x}$ is the state vector, $\mathbf{u}_k \in U \subset \mathbb{R}^{m_u}$ is the control vector, $\dot{\mathbf{x}}_k \in \mathbb{R}^{m_x}$ is the time derivative of state vector, and $\mathbf{f} : \mathbb{R}^{m_x} \mapsto \mathbb{R}^{m_u}$ is the dynamic model. We assume the legal state set X and control set U are both defined by linear constraints, which covers most cases in practice.

In the NNDM case, the dynamic model \mathbf{f} is encoded by a n -layer feedforward neural network. Each layer in \mathbf{f} corresponds to a function $\mathbf{f}_i : \mathbb{R}^{k_{i-1}} \mapsto \mathbb{R}^{k_i}$, where k_i is the dimension of the hidden variable \mathbf{z}_i in layer i , and $k_0 = m_x + m_u$, $k_n = m_x$. Hence, the network can be represented by $\mathbf{f} = \mathbf{f}_n \circ \mathbf{f}_{n-1} \circ \dots \circ \mathbf{f}_1$. The function at layer i is $\mathbf{z}_i = \mathbf{f}_i(\mathbf{z}_{i-1}) = \sigma_i(\hat{\mathbf{z}}_i) = \sigma_i(\mathbf{W}_i \mathbf{z}_{i-1} + \mathbf{b}_i)$ where $\mathbf{W}_i \in \mathbb{R}^{k_i \times k_{i-1}}$ is the weight matrix, $\mathbf{b}_i \in \mathbb{R}^{k_i}$ is the bias vector, and $\sigma_i : \mathbb{R}^{k_i} \mapsto \mathbb{R}^{k_i}$ is the activation function. We only consider ReLU activation in this work. For simplicity, denote $\mathbf{W}_i \mathbf{z}_{i-1} + \mathbf{b}_i$ by $\hat{\mathbf{z}}_i$. Let $z_{i,j}$ be the value of the j^{th} node in the i^{th} layer, $\mathbf{w}_{i,j} \in \mathbb{R}^{1 \times k_{i-1}}$ be the j^{th} row in \mathbf{W}_i , and $b_{i,j}$ be the j^{th} entry in \mathbf{b}_i .

Safety constraint We consider the safety specification as a requirement that the system state should be constrained in a connected and closed set $\mathcal{X} \subseteq \mathbb{R}^{m_x}$ which is called the safe set. \mathcal{X} should be a zero-sublevel set of a safety index function $\phi_0 : X \mapsto \mathbb{R}$, *i.e.*

$$\mathcal{X} = \{\mathbf{x} \mid \phi_0(\mathbf{x}) \leq 0\}. \quad (2)$$

There can be many different definitions of ϕ_0 for a given \mathcal{X} . Ideally, a safe control law should guarantee forward invariance, *i.e.* $\phi_0(\mathbf{x}_k) \leq 0 \implies \phi_0(\mathbf{x}_{k+1}) \leq 0$. And when the state is unsafe, a safe control law should drive the system back to the safe set \mathcal{X} . One way is to make \mathcal{X} the region of attraction (ROA) of the whole space [5]: $\phi_0(\mathbf{x}_k) > 0 \implies \phi_0(\mathbf{x}_{k+1}) \leq \phi_0(\mathbf{x}_k) - \gamma dt$. These two conditions form the safety constraint in the discrete time:

$$\phi_0(\mathbf{x}_{k+1}) \leq \max\{0, \phi_0(\mathbf{x}_k) - \gamma dt\}, \quad (3)$$

Feasibility However, not all $\mathbf{x}_k \in \mathcal{X}$ has a safe control $\mathbf{u}_k \in U$ that satisfies eq. (3). For example, if ϕ_0 measures the distance between the ego vehicle and the leading vehicle. It is possible that the ego is still far from the leading vehicle ($\phi_0(\mathbf{x}_k) < 0$), but the relative speed is too high, the collision is unavoidable ($\phi_0(\mathbf{x}_{k+1}) > 0$). We define the collection of these inevitable states as \mathcal{X}_d :

$$\mathcal{X}_d(\phi_0) = \{\mathbf{x} \mid \phi_0(\mathbf{x} + \mathbf{f}(\mathbf{x}, \mathbf{u})dt) > \max\{0, \phi_0(\mathbf{x}) - \gamma dt\}, \forall \mathbf{u} \in U\}. \quad (4)$$

The set \mathcal{X}_d can be nonempty when the relative degree from ϕ_0 to \mathbf{u} is greater than one or when the control inputs are bounded. In these cases, \mathcal{X} may not be forward invariant or globally attractive. To address this problem, we want to find a subset $\mathcal{X}_s \subseteq \mathcal{X}$ and choose a control law to make the subset forward invariant and have finite time convergence. This subset is called a control invariant set.

When we use analytical models, we can manually craft a \mathcal{X}_s by designing a safety index ϕ that minimizes the size of $\mathcal{X}_d(\phi)$ [4]. However, it is challenging to manually design \mathcal{X}_s for NNDM due to the poor interpretability of neural networks.

The safe tracking problem This paper considers the following constrained optimization for safe tracking:

$$\begin{aligned} \min_{\mathbf{u}_k, \mathbf{x}_{k+1}} \quad & \|\mathbf{x}_{k+1} - \mathbf{x}_{k+1}^r\|_p \\ \text{s.t.} \quad & \mathbf{x}_{k+1} = \mathbf{x}_k + \mathbf{f}(\mathbf{x}_k, \mathbf{u}_k)dt, \quad \mathbf{u}_k \in U \\ & \phi_0(\mathbf{x}_{k+1}) \leq \max\{0, \phi_0(\mathbf{x}_k) - \gamma dt\} \end{aligned} \quad (5)$$

where $\|\cdot\|_p$ can be either ℓ_1 -norm or ℓ_2 -norm. This formulation is essentially a one-step model predictive control (MPC). The extension to multi-step MPC is straightforward, which we leave for future work. At a given step k , (5) is a nonlinear programming problem. However, existing nonlinear solvers have poor performance on neural networks (which will be shown in section 5). That is because neural networks are piece-wise linear, whose second-order derivatives are not informative. New techniques are needed to solve this problem efficiently.

3 Related work

Optimization with Neural Network Constraints Recent progress in nonlinear optimization involving neural network constraints can be classified as primal optimization methods and dual optimization methods. The primal optimization methods encode the nonlinear activation functions (e.g., ReLU) as mixed-integer linear programmings [11, 12], relaxed linear programmings [13] or semidefinite programmings [14]. Dual optimization methods simplify the constraints by directly solving the Lagrangian of the optimization [15–17]. These methods are mostly designed for checking input-output constraints, that is, given an input constraint, whether all the output of the neural network complies with some output constraints. Therefore, not all the methods are designed to minimize an objective. And some methods are not complete, they may not return a valid solution even there is one. Our proposed method to encode NNDM is inspired by MIPVerify [11], which uses mixed integer programming to compute maximum allowable disturbances to the input. MIPVerify is complete and sound, *i.e.*, it can always find the solution if there is one, and the solution is always correct. We also discuss the potential application of approximate verification method in appendix A.9.

QP-based safe control When the system dynamics are analytical and control-affine, the safe tracking problem can be decomposed into two steps: 1) computing a reference control \mathbf{u}^r by model inverse; 2) finding a safe control that complies with the constraints in (5) but minimizes the distance to the reference control, *i.e.* $\min_{\mathbf{u}_k} \|\mathbf{u}_k - \mathbf{u}_k^r\|$. For analytical control-affine dynamic models, the set of safe control that satisfies the constraints in (5) is a half-space intersecting with U . Therefore, the second step is essentially a quadratic projection of the reference control to that linear space, which can be efficiently computed by calling a quadratic programming (QP) solver. Existing methods include CBF-QP [5], SSA-QP [18], etc. However, to our best knowledge, there has not been any quadratic projection method that projects a reference control to a safety constraint with non-analytical (non-control-affine) dynamic models. Moreover, our work solves both steps in an integrated manner, which is not limited to the quadratic projection of the reference control.

Persistent feasibility in MPC There are different approaches in MPC literature to compute the control invariant set to ensure persistent feasibility, such as Lyapunov function [19], linearization-convexification [20] and grid-based reachability analysis [21]. However, most of the non-grid-based methods approximate the control invariant set as intersection or union of linear constraints, which greatly limit the expressiveness of the geometries. Although grid-based methods have better expressiveness and may be able to extend to non-analytical models, they have limited scalability due to the curse of dimensionality. Our method can synthesize the control invariant set with nonlinear boundaries for non-analytical models.

4 Method

In this section, we discuss how to efficiently solve the constrained optimization (5) and ensure it is persistently feasible. First, we introduce MIND, a way to find the optimal control by encoding NNNDM constraints as mixed integer constraints. Then we present SIS, a method to find the control invariant set by learning a new safety index ϕ that minimizes the size of $\mathcal{X}_d(\phi)$ in (4). Finally, we present the reformulated problem.

4.1 MIND: Encode NNNDM constraints

To overcome the complexity of NNNDM constraints, we first add all hidden nodes in the neural network as decision variables and turn (5) into the following equivalent form:

$$\begin{aligned} \min_{\mathbf{u}_k, \mathbf{x}_{k+1}, \mathbf{z}_i} \quad & \|\mathbf{x}_{k+1} - \mathbf{x}_{k+1}^r\|_p \\ \text{s.t.} \quad & \mathbf{x}_{k+1} = \mathbf{x}_k + \mathbf{z}_n dt, \mathbf{z}_0 = [\mathbf{x}_k, \mathbf{u}_k], \quad \mathbf{u}_k \in U \\ & z_{i,j} = \max\{\hat{z}_{i,j}, 0\}, \hat{z}_{i,j} = \mathbf{w}_{i,j} \mathbf{z}_{i-1} + b_{i,j}, \forall i \in \{1, \dots, n\}, \forall j \in \{1, \dots, k_i\} \\ & \phi_0(\mathbf{x}_{k+1}) \leq \max\{0, \phi_0(\mathbf{x}_k) - \gamma dt\}. \end{aligned} \quad (6)$$

Nevertheless, the nonlinear non-smooth constraints introduced by the ReLU activation $z_{i,j} = \max\{\hat{z}_{i,j}, 0\}$ in (6) is still challenging to handle. Inspired by MIPVerify [11], we use mixed integer formulation to rewrite these constraints. We first introduce an auxiliary variable $\delta_{i,j}$ to denote the activation status of the ReLU node:

$$\delta_{i,j} = 1 \Rightarrow z_{i,j} = \hat{z}_{i,j}, \quad \delta_{i,j} = 0 \Rightarrow z_{i,j} = 0. \quad (7)$$

Then we compute the pre-activation upper bounds $\hat{u}_{i,j}$ and lower bound $\hat{l}_{i,j}$ of every node in the neural network using interval arithmetics [22]. Given the ranges of variables (e.g., $x \in [1, 2]$ and $y \in [3, 4]$), interval arithmetic computes the output range using the lower and upper bounds (e.g., $x - y \in [1 - 4, 2 - 3] = [-3, -1]$). When $\hat{u}_{i,j} \leq 0$, the constraint for ReLU activation reduces to $z_{i,j} = 0$. When $\hat{l}_{i,j} \geq 0$, the constraint reduces to $z_{i,j} = \hat{z}_{i,j}$. Otherwise, the constraint can be represented as the following linear inequalities:

$$z_{i,j} \geq \hat{z}_{i,j}, z_{i,j} \geq 0, z_{i,j} \leq \hat{z}_{i,j} - \hat{l}_{i,j} (1 - \delta_{i,j}), z_{i,j} \leq \hat{u}_{i,j} \delta_{i,j}, \delta_{i,j} \in \{0, 1\}. \quad (8)$$

With this encoding, the constrained optimization is converted into a MIP, which can be efficiently solved by existing solvers. But the safety constraint may be violated during execution due to infeasibility. An example is shown in fig. 2. Therefore, we introduce SIS.

4.2 SIS: Guarantee feasibility

The goal of safety index synthesis is to find a safety index that guarantees both safety and feasibility. We do this by synthesizing a safety index ϕ that minimizes the size of the inevitable states set $\mathcal{X}_d(\phi)$. [4] gives a form of ϕ that can improve feasibility, $\phi(\mathbf{x}) = \phi_0^*(\mathbf{x}) + \sum p_i(\alpha_i, \mathbf{x}) + \beta$, where $\phi_0^*(\mathbf{x})$ defines the same sublevel set as ϕ_0 , $p_i(\alpha_i, \mathbf{x})$ is a higher order term of ϕ_0 that is parameterized by α_i , and β is a constant. The choice of ϕ_0^* , p_i and β depends on the system. We prove that this form guarantees safety in appendix A.3.

The problem can be formulated as $\min_{\alpha, \beta, \gamma} |\mathcal{X}_d|$ where γ is from (3). Because the gradient from $|\mathcal{X}_d|$ to α, β, γ is usually difficult to compute. So we use a derivative-free evolutionary approach, CMA-ES [23] to learn the parameters. CMA-ES runs for multiple generations. In each generation, the algorithm samples many parameter candidates, which are called members, from a multi-variant Gaussian distribution and evaluates their performance. Then some of the candidates with the best performance will be used to update the mean and variance of the Gaussian distribution. To evaluate whether a set of parameters minimizes the number of inevitable states, we uniformly sample from the state space and check whether the safe control set for each state sample is empty.

We prove that as long as the sampling is dense enough, we can guarantee the learned safety index is feasible for an arbitrary state. The proof of the following lemma is in appendix A.2.

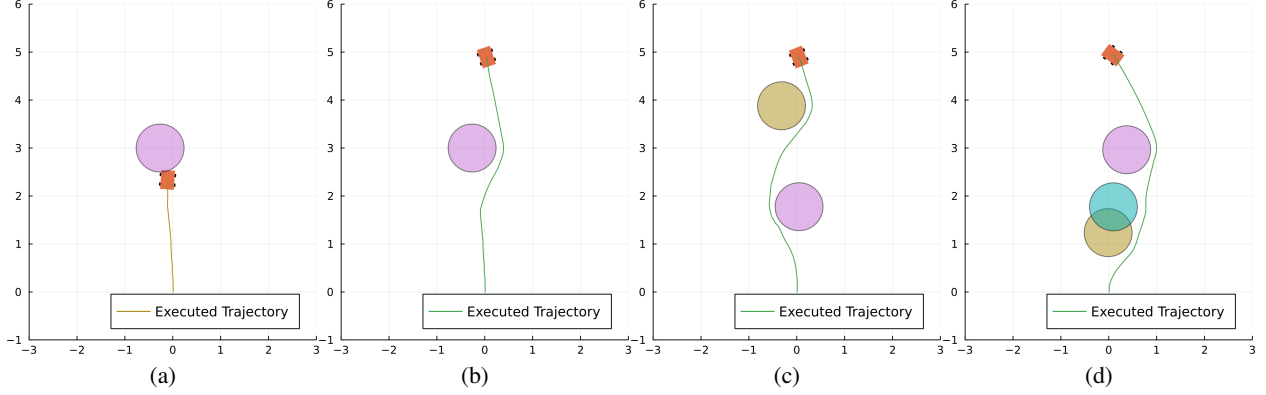


Figure 2: MIND-SIS in collision avoidance. (a) shows the trajectory with ϕ_0 . The vehicle collides with the obstacle because of infeasibility (too late to break). (b) (c) (d) show the trajectories with a synthesized safety index ϕ in different scenarios. The synthesized safety index is general enough so that it can be directly applied to scenarios with multiple obstacles without any modification.

Lemma 4.1. Suppose we sample a state subset $S \subset X$ such that $\forall \mathbf{x} \in X, \min_{\mathbf{x}' \in S} \|\mathbf{x} - \mathbf{x}'\| \leq \delta$. And if $\forall \mathbf{x}' \in S, \exists \mathbf{u}$, s.t. $\phi(\mathbf{x}' + \mathbf{f}(\mathbf{x}', \mathbf{u})dt) \leq \max\{-\epsilon, \phi(\mathbf{x}') - (\gamma + \epsilon)dt\}$ where $\epsilon = k_\phi(k_f + 2)\delta$, k_f and k_ϕ are the Lipschitz constants of \mathbf{f} and ϕ . Then $\forall \mathbf{x} \in X, \exists \mathbf{u}$, s.t.

$$\phi(\mathbf{x} + \mathbf{f}(\mathbf{x}, \mathbf{u})dt) \leq \max\{0, \phi(\mathbf{x}) - \gamma dt\}. \quad (9)$$

4.3 MIND-SIS: Safe control with NNDM

Once the safety index is synthesized, we substitute ϕ_0 with ϕ in (6) to guarantee the feasibility. To address the nonlinearity in the safety constraint (3), we approximate it with first order Taylor expansion at the current state \mathbf{x}_k (appendix A.1 discusses how the safety guarantee is preserved):

$$\phi(\mathbf{x}_{k+1}) = \phi(\mathbf{x}_k) + \nabla_{\mathbf{x}}\phi \cdot \mathbf{f}(\mathbf{x}_k, \mathbf{u}_k)dt + o(\|\mathbf{f}(\mathbf{x}_k, \mathbf{u}_k)dt\|), \quad (10)$$

where $\lim_{dt \rightarrow 0} o(\|\mathbf{f}(\mathbf{x}_k, \mathbf{u}_k)dt\|) = 0$. Then (6) is transformed into the following mixed integer problem:

$$\begin{aligned} \min_{\mathbf{u}_k, \mathbf{x}_{k+1}, \mathbf{z}_i, \delta_{i,j} \in \{0,1\}} & \|\mathbf{x}_{k+1} - \mathbf{x}_{k+1}^r\|_p \\ \text{s.t. } & \mathbf{x}_{k+1} = \mathbf{x}_k + \mathbf{z}_n dt, \mathbf{z}_0 = [\mathbf{x}_k, \mathbf{u}_k], \quad \mathbf{u}_k \in U, \\ & z_{i,j} \geq \hat{z}_{i,j}, z_{i,j} \geq 0, z_{i,j} \leq \hat{z}_{i,j} - \hat{\ell}_{i,j}(1 - \delta_{i,j}), z_{i,j} \leq \hat{u}_{i,j}\delta_{i,j}, \\ & \hat{z}_{i,j} = \mathbf{w}_{i,j}\mathbf{z}_{i-1} + b_{i,j}, \forall i \in \{1, \dots, n\}, \forall j \in \{1, \dots, k_i\} \\ & \nabla_{\mathbf{x}}\phi \cdot \mathbf{f}(\mathbf{x}_k, \mathbf{u}_k) \leq \max\left\{-\frac{\phi(\mathbf{x}_k)}{dt}, -\gamma\right\}. \end{aligned} \quad (11)$$

Depending on the norm $\|\cdot\|_p$, eq. (11) is either a Mixed Integer Linear Programming or Quadratic Programming, which both can be solved by existing solvers, such as GLPK, CPLEX, and Gurobi.

5 Experiment

5.1 Experiment set up

The evaluation is designed to answer the following questions:

1. How does our method (by solving (11)) compare to the shooting method and regular nonlinear solvers on the original problem (5) in terms of optimality and computational efficiency?
2. Does the safety index synthesis improve persistent feasibility?
3. Does our method ensure safety in terms of forward invariance and finite-time convergence?

We evaluate our method on a system with vehicle NNDMs. The NNDMs are learned from a unicycle dynamic model with 4 state input, 2 control inputs, and 4 state outputs. We learn 3 different NNDMs to show the generalizability

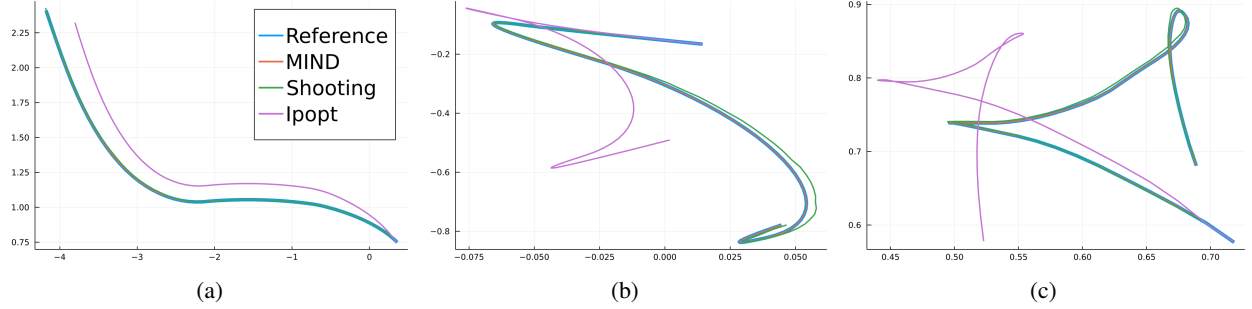


Figure 3: Illustration of trajectory tracking with NNDM using different optimization methods: MIND (our method), shooting method with sample size of 100, and Ipopt. (a-c) show 3 randomly generated trajectories. MIND has the smallest tracking error in all three cases.

of our method, which are: I. 3-layer fully connected network with 50 hidden neurons each layer. II. 3-layer fully connected network with 100 hidden neurons each layer. III. 4-layer fully connected network with 50 hidden neurons each layer. Scalability analysis with more models can be found in appendix A.6.

After the learning, we use the NNDM to directly control the agent to avoid model mismatch in our evaluation. The mismatch between the learned model and the actual dynamics can be caused by simplification, system noises, insufficient learning, etc. The safe control computed by the learned model may be unsafe for the actual dynamics when there is model mismatch. A study is shown in appendix A.7. Our evaluation aims to show that the proposed method can give provably safe controls efficiently under the NNDM. As future work, we will extend our work to robust safe control, which can guarantee safety even with model mismatch [24, 25].

To answer the questions we raised in the beginning, we design the following two tasks. The first task is trajectory tracking without safety constraints, which can test how our method performs comparing to other methods in terms of optimality and computational efficiency. And the second task is trajectory tracking under safety constraints. It is to test whether the learned safety index improves the feasibility and whether MIND-SIS ensures forward invariance and finite time convergence.

Method	NNDM 1			NNDM 2			NNDM 3		
	Mean	Std	Time (s)	Mean	Std	Time (s)	Mean	Std	Time (s)
MIND	$< 10^{-8}$	$< 10^{-7}$	36.4	$< 10^{-8}$	$< 10^{-7}$	83.8	$< 10^{-8}$	$< 10^{-7}$	123.5
Shooting- 10^3	0.129	0.080	2.1	0.128	0.080	10.0	0.128	0.080	2.9
Shooting- 10^4	0.041	0.026	20.9	0.041	0.026	100.2	0.041	0.026	28.3
Shooting- 10^5	0.012	0.007	208.4	0.012	0.007	1006.3	0.012	0.007	282.2
Ipopt	1.871	0.626	3.2	1.852	0.619	4.0	1.865	0.623	3.3
Ipopt-iterative	1.871	0.626	13.3	1.852	0.619	16.3	1.865	0.623	13.5

Table 1: Average tracking error and computation time for different methods in the trajectory tracking task (without safety constraint). The table shows mean and standard deviation of the average tracking error. The number after “Shooting” denotes the sampling size. “Ipopt-iterative” represents iteratively solving the problem by warm starting Ipopt with its own solution. Our method can always find the optimal solution, therefore achieves almost zero tracking error. The actual trajectories are illustrated in fig. 3.

5.2 Trajectory tracking

In this task, we randomly generate 500 reference trajectory waypoints that are dynamically feasible for each NNDM. We compare our method with shooting methods with different sampling sizes and Ipopt (short for Interior Point OPTimizer), a popular nonlinear solver. We use CPLEX to solve the MIND-SIS formulation. This experiment is done on a computer with AMD® Ryzen threadripper 3960x 24-core processor, 128 GB memory. Some results are shown in fig. 3. Detailed settings and comparison of control sequences can be found in appendix A.5.

As shown in table 1, MIND achieves an average tracking error less than 10^{-8} . The tracking error is less than the resolution of single-precision floats. We can consider MIND finds the optimal solution, which is a significant improvement comparing to other methods. The shooting method achieves lower tracking error with a larger sampling size but also takes a longer time. To achieve the same tracking error as MIND, the sampling size and computation time will be unacceptably large. Ipopt ends quickly because it gets stuck at local optima soon after the beginning. And iteratively

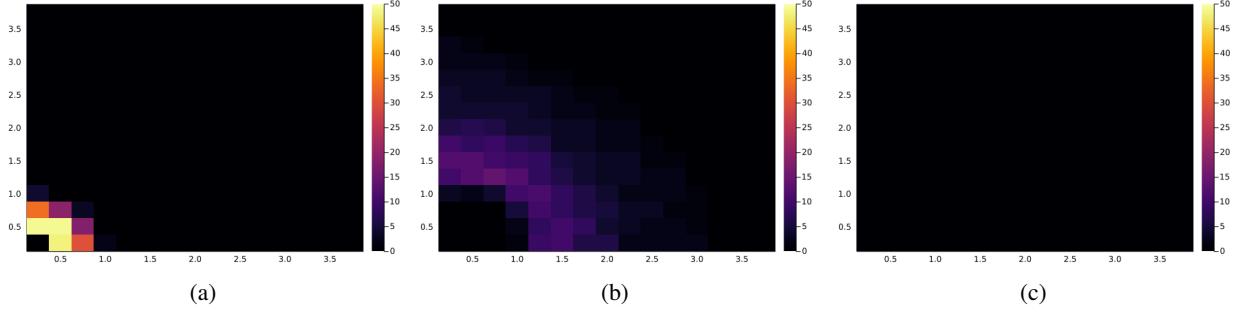


Figure 4: Inevitable states distribution. An obstacle is located at $(0, 0)$. Each grid in the graph corresponds to a (p_x, p_y) location. We sample 100 states at each location. The color denote how many states at this location are inevitable states. (a) shows the original safety index ϕ_0 has a hard boundary, which means when the agent is near the obstacle, no matter with what state, it can barely find a feasible control. (b) shows a hand constructed safety index ϕ^h only can not find a feasible control for part of the states around the obstacle. (c) shows the learned index ϕ has no inevitable state, thus can always find a safe control.

warm starting Ipopt with its own solution does not help it get out of local optima. This suggests existing nonlinear solvers do not work well with neural network constraints.

5.3 Trajectory tracking under safety constraints

This task considers two safety constraints corresponding to different scenarios: collision avoidance and safe following. When infeasibility happens, the agent reuses the control of the last time step.

5.3.1 Collision avoidance

Collision avoidance is one of the most common requirement in real-world applications, such as in vehicle driving, flight control [26], and robot operation [27]. The collision avoidance constraint is usually defined as $\phi_0(\mathbf{x}) = d_{min} - d(\mathbf{x}) < 0$, where d_{min} is the acceptable minimal distance between the agent and the obstacle, $d(\mathbf{x})$ is the relative distance from the agent to the obstacle. But this constraint usually can not guarantee persistent feasibility. Therefore, we synthesize a safety index $\phi(\mathbf{x})$ that guarantees persistent feasibility. We design the safety constraint to be of the form:

$$\phi(\mathbf{x}) = d_{min}^{\alpha_1} - d(\mathbf{x})^{\alpha_1} - \alpha_2 \dot{d}(\mathbf{x}) + \beta,$$

where $\dot{d}(\mathbf{x})$ is the relative velocity from the agent to the obstacle, α_1 , α_2 and β are parameters to learn. This form guarantees forward invariance and finite time convergence as shown in [4], which will be discussed in more details in appendix A.3. To demonstrate the effect of the synthesized safety index. We visualize the behavior of the agent with ϕ_0 and ϕ in fig. 2. The figure also shows that the synthesized safety index can be directly applied to unseen multi-obstacle scenarios without any change. Although, multi-obstacle may cause deadlock problems as discussed in appendix A.4.

We use CMA-ES to optimize the parameters to learn a persistent feasible safety index. The search range for each parameters is: $\gamma \in (0.001, 0.02)$, $\alpha_1 \in (0, 3)$, $\alpha_2 \in (0, 10)$, $\beta \in (0.1, 0.5)$. For each set of parameters, we test how many sampled states are inevitable. We place an obstacle at $(0, 0)$, and uniformly sample 40000 states around the obstacle. Then compute whether the control set of each state is empty. fig. 4 shows the distribution of inevitable states of the original safety index ϕ_0 , a synthesized safety index ϕ^h with parameters given by previous work [4], and a synthesized safety index ϕ^l with learned parameters. The learned safety index ϕ^l has no inevitable states, thus can always find a safe control. Additional comparison of safety indexes is in appendix A.8.

We evaluate these safety indexes on 100 randomly generated collision avoidance tasks. The agent has to track a trajectory in each task while avoiding collision (keep $\phi_0 \leq 0$). We consider a task succeeds if there is no collision or inevitable states on the trajectory. The evaluation results are shown in table 2. We can see that the learned safety index achieves 0% ϕ_0 -violation rate and 0% infeasible rate.

5.3.2 Safe following

The safe following constraint appears when an agent is following a target while keeping a safe distance, such as in adaptive cruise control, nap-of-the-earth flying, etc. The safety index can be defined as $\phi_0(\mathbf{x}) = (d(\mathbf{x}) - d_{min})(d(\mathbf{x}) -$

Metric	Collision avoidance			Safe following		
	ϕ_0	ϕ^h	ϕ^l	ϕ_0	ϕ^h	ϕ^l
Success rate	0%	72%	100%	0%	82%	100%
ϕ_0 -violation rate	100%	0%	0%	100%	0%	0%
Infeasible rate	100%	28%	0%	100%	18%	0%

Table 2: Performance comparison of the original safety index ϕ_0 , a synthesized safety index ϕ^h with manually tuned parameters, and a synthesized safety index ϕ^l with learned parameters on 100 randomly generated tasks. We consider one trial successful if there is no safety violation or infeasible state. We can see that ϕ_0 always violates the constraints due to infeasibility (due to our choice of the initial state). ϕ^h guarantees the safety but fail to find controls for some states due to infeasibility. But the learned index ϕ^l can always find a control and guarantees safety.

d_{max}). We design the safety constraint to be of the form:

$$\phi(\mathbf{x}) = (d(\mathbf{x}) - d_{min})^{\alpha_1} (d(\mathbf{x}) - d_{max})^{\alpha_1} + \alpha_2 [d(\mathbf{x})\dot{d}(\mathbf{x}) + \dot{d}(\mathbf{x})(d_{min} + d_{max})] + \beta \quad (12)$$

Where $\alpha_1, \alpha_2, \beta$ are parameters to learn, The learning process is the same as the collision avoidance case. The search range is $\gamma \in (0.001, 1)$, $\alpha_1 \in \{1, 3\}$, $\alpha_2 \in (0, 10)$, $\beta \in (0.01, 0.5)$. We also randomly generate 100 following tasks for evaluation. We consider a task successful if there is no ϕ_0 constraint violation or infeasible state during the following. The evaluation results are shown in table 2. The learned index achieves 0% ϕ_0 -violation rate and 0% infeasible rate.

6 Discussion

In this work, we propose MIND-SIS, the first method to derive safe control law for NNDM. MIND provides a way to find the optimal control for NNDM, and SIS can synthesize a safety index that guarantees forward invariance and finite time convergence. We provide theoretical guarantees that our method can achieve optimality and ensure feasibility.

The synthesized safety index guarantees feasibility, but the efficiency of the system may not be maximized. How to improve the efficiency of the system on top of safety is an interesting question for future exploration.

Safe control with NNDM can improve the system safety even if the NNDM is not perfectly learned. However, safety violation may still exist due to model mismatch. We will explore how to quantify the model mismatch and guarantee safety under model mismatch in the future.

References

- [1] M. Nagumo, “Über die lage der integralkurven gewöhnlicher differentialgleichungen,” *Proceedings of the Physico-Mathematical Society of Japan. 3rd Series*, vol. 24, pp. 551–559, 1942.
- [2] F. Blanchini, “Set invariance in control,” *Automatica*, vol. 35, no. 11, pp. 1747–1767, 1999.
- [3] T. Wei and C. Liu, “Safe control algorithms using energy functions: A uni ed framework, benchmark, and new directions,” in *2019 IEEE 58th Conference on Decision and Control (CDC)*. IEEE, 2019, pp. 238–243.
- [4] C. Liu and M. Tomizuka, “Control in a safe set: Addressing safety in human-robot interactions,” in *ASME 2014 Dynamic Systems and Control Conference*. American Society of Mechanical Engineers Digital Collection, 2014.
- [5] A. D. Ames, X. Xu, J. W. Grizzle, and P. Tabuada, “Control barrier function based quadratic programs for safety critical systems,” *IEEE Transactions on Automatic Control*, vol. 62, no. 8, pp. 3861–3876, 2016.
- [6] D. Nguyen-Tuong and J. Peters, “Model learning for robot control: a survey,” *Cognitive processing*, vol. 12, no. 4, pp. 319–340, 2011.
- [7] A. Nagabandi, G. Kahn, R. S. Fearing, and S. Levine, “Neural network dynamics for model-based deep reinforcement learning with model-free fine-tuning,” in *2018 IEEE International Conference on Robotics and Automation (ICRA)*. IEEE, 2018, pp. 7559–7566.
- [8] M. Janner, J. Fu, M. Zhang, and S. Levine, “When to trust your model: Model-based policy optimization,” *arXiv preprint arXiv:1906.08253*, 2019.
- [9] D. Tolani, A. Goswami, and N. I. Badler, “Real-time inverse kinematics techniques for anthropomorphic limbs,” *Graphical models*, vol. 62, no. 5, pp. 353–388, 2000.

- [10] C. Liu, T. Arnon, C. Lazarus, C. Strong, C. Barrett, M. J. Kochenderfer *et al.*, “Algorithms for verifying deep neural networks,” *Foundations and Trends® in Optimization*, vol. 4, 2020.
- [11] V. Tjeng, K. Xiao, and R. Tedrake, “Evaluating robustness of neural networks with mixed integer programming,” *arXiv preprint arXiv:1711.07356*, 2017.
- [12] A. Lomuscio and L. Maganti, “An approach to reachability analysis for feed-forward relu neural networks,” *arXiv preprint arXiv:1706.07351*, 2017.
- [13] R. Ehlers, “Formal verification of piece-wise linear feed-forward neural networks,” in *International Symposium on Automated Technology for Verification and Analysis*. Springer, 2017, pp. 269–286.
- [14] A. Raghunathan, J. Steinhardt, and P. Liang, “Semidefinite relaxations for certifying robustness to adversarial examples,” p. 11.
- [15] K. Dvijotham, R. Stanforth, S. Gowal, T. A. Mann, and P. Kohli, “A dual approach to scalable verification of deep networks,” in *UAI*, vol. 1, no. 2, 2018, p. 3.
- [16] E. Wong and Z. Kolter, “Provable defenses against adversarial examples via the convex outer adversarial polytope,” in *International Conference on Machine Learning*. PMLR, 2018, pp. 5286–5295.
- [17] S. Dathathri, K. Dvijotham, A. Kurakin, A. Raghunathan, J. Uesato, R. Bunel, S. Shankar, J. Steinhardt, I. Goodfellow, P. Liang *et al.*, “Enabling certification of verification-agnostic networks via memory-efficient semidefinite programming,” *arXiv preprint arXiv:2010.11645*, 2020.
- [18] C. Liu, C.-Y. Lin, and M. Tomizuka, “The convex feasible set algorithm for real time optimization in motion planning,” *SIAM Journal on Control and optimization*, vol. 56, no. 4, pp. 2712–2733, 2018.
- [19] C. Danielson, A. Weiss, K. Berntorp, and S. Di Cairano, “Path planning using positive invariant sets,” in *2016 IEEE 55th Conference on Decision and Control (CDC)*. IEEE, 2016, pp. 5986–5991.
- [20] M. Jalalmaab, B. Fidan, S. Jeon, and P. Falcone, “Guaranteeing persistent feasibility of model predictive motion planning for autonomous vehicles,” in *2017 IEEE Intelligent Vehicles Symposium (IV)*. IEEE, 2017, pp. 843–848.
- [21] S. Bansal, M. Chen, S. Herbert, and C. J. Tomlin, “Hamilton-jacobi reachability: A brief overview and recent advances,” in *2017 IEEE 56th Annual Conference on Decision and Control (CDC)*. IEEE, 2017, pp. 2242–2253.
- [22] R. E. Moore, R. B. Kearfott, and M. J. Cloud, *Introduction to interval analysis*. SIAM, 2009.
- [23] N. Hansen, “The cma evolution strategy: A tutorial,” *arXiv preprint arXiv:1604.00772*, 2016.
- [24] C. Liu and M. Tomizuka, “Safe exploration: Addressing various uncertainty levels in human robot interactions,” in *2015 American Control Conference (ACC)*. IEEE, 2015, pp. 465–470.
- [25] C. Noren and C. Liu, “Safe adaptation in confined environments using energy functions,” *arXiv preprint arXiv:1912.09095*, 2019.
- [26] A. Platzer and E. M. Clarke, “Formal verification of curved flight collision avoidance maneuvers: A case study,” in *International Symposium on Formal Methods*. Springer, 2009, pp. 547–562.
- [27] H.-C. Lin, C. Liu, Y. Fan, and M. Tomizuka, “Real-time collision avoidance algorithm on industrial manipulators,” in *2017 IEEE Conference on Control Technology and Applications (CCTA)*. IEEE, 2017, pp. 1294–1299.
- [28] Gurobi Optimization, LLC, “Gurobi Optimizer Reference Manual,” 2021. [Online]. Available: <https://www.gurobi.com>

A Appendices

A.1 Continuous time vs discrete time safe control

Our work is formulated in discrete time. There are vast literature dealing with safe control in continuous time. The major difference lies in the formulation of constraints. While our constraint is formulated as in (3), the constraint for continuous time safe control is formulated as $\dot{\phi} \leq -\kappa(\phi)$ where κ is a non decreasing function where $\kappa(0) \geq 0$. In CBF, κ is chosen as $\kappa = \lambda\phi$. In SSA, κ is chosen as γ when $\phi \geq 0$ and $-\infty$ when $\phi < 0$. Our method can be easily extend to continuous time safe control since $\dot{\phi}(\mathbf{x}_k) \approx (\phi(\mathbf{x}_{k+1}) - \phi(\mathbf{x}_k))/dt$.

Due to discrete time control, we approximate the safety constraints with first order Taylor expansion in (10). The error caused by omitting higher order terms can be bounded by introducing a constant safety margin [4] $\lambda = c\|\dot{\mathbf{x}}\|_{\max}dt$, where c is a constant, $\|\dot{\mathbf{x}}\|_{\max}$ is the possible maximum norm of $\dot{\mathbf{x}}$, which can be found by solving the MIP formulation with whole state space and whole control space as input constraints. We set the lower bound of β as the safety margin to ensure the safety in our work. In this way, we can make sure the safe control set found in the discrete case is a subset of safe control set in continuous case, therefore the safety is guaranteed.

A.2 Proof for Lemma 4.1 in safety index synthesis

Proof. We proof the claim in Lemma 4.1 by breaking it into two cases and proving each case separately.

Case 1. We prove that if $\exists \mathbf{u}, s.t. \phi(\mathbf{x}' + \mathbf{f}(\mathbf{x}', \mathbf{u})dt) < -\epsilon_1$, then $\phi(\mathbf{x} + \mathbf{f}(\mathbf{x}, \mathbf{u})dt) < 0$

$$\phi(\mathbf{x} + \mathbf{f}(\mathbf{x}, \mathbf{u})dt) = \phi(\mathbf{x} + \mathbf{f}(\mathbf{x}, \mathbf{u})dt) - \phi(\mathbf{x}' + \mathbf{f}(\mathbf{x}', \mathbf{u})dt) + \phi(\mathbf{x}' + \mathbf{f}(\mathbf{x}', \mathbf{u})dt) \quad (13)$$

$$\leq k_\phi \|\mathbf{x} - \mathbf{x}' + \mathbf{f}(\mathbf{x}, \mathbf{u}) - \mathbf{f}(\mathbf{x}', \mathbf{u})\| - \epsilon_1 \quad (14)$$

$$\leq k_\phi \|\mathbf{x} - \mathbf{x}'\| + k_\phi \|\mathbf{f}(\mathbf{x}, \mathbf{u}) - \mathbf{f}(\mathbf{x}', \mathbf{u})\| - \epsilon_1 \quad (15)$$

$$\leq k_\phi \delta + k_\phi k_f \delta - \epsilon_1 \quad (16)$$

$$\leq k_\phi(k_f + 1)\delta - \epsilon_1 \quad (17)$$

$$\leq 0 \quad (18)$$

Case 2. We prove that if $\exists \mathbf{u}, s.t. \phi(\mathbf{x}' + \mathbf{f}(\mathbf{x}', \mathbf{u})dt) \leq \phi(\mathbf{x}') - (\gamma + \epsilon_2)dt$, then $\phi(\mathbf{x} + \mathbf{f}(\mathbf{x}, \mathbf{u})dt) \leq \phi(\mathbf{x}) - \gamma dt$

$$\phi(\mathbf{x} + \mathbf{f}(\mathbf{x}, \mathbf{u})dt) - \phi(\mathbf{x}) + \gamma dt \quad (19)$$

$$= \phi(\mathbf{x} + \mathbf{f}(\mathbf{x}, \mathbf{u})dt) - \phi(\mathbf{x}' + \mathbf{f}(\mathbf{x}', \mathbf{u})) + \phi(\mathbf{x}' + \mathbf{f}(\mathbf{x}', \mathbf{u})) - \phi(\mathbf{x}) + \gamma dt \quad (20)$$

$$\leq k_\phi \|\mathbf{x} - \mathbf{x}' + \mathbf{f}(\mathbf{x}, \mathbf{u}) - \mathbf{f}(\mathbf{x}', \mathbf{u})\| + \phi(\mathbf{x}' + \mathbf{f}(\mathbf{x}', \mathbf{u})) - \phi(\mathbf{x}') + \phi(\mathbf{x}') - \phi(\mathbf{x}) + \gamma dt \quad (21)$$

$$\leq k_\phi(k_f + 1)\delta + [\phi(\mathbf{x}' + \mathbf{f}(\mathbf{x}', \mathbf{u})) - \phi(\mathbf{x}') + \gamma dt] + \phi(\mathbf{x}') - \phi(\mathbf{x}) \quad (22)$$

$$\leq k_\phi(k_f + 1)\delta + \epsilon_2 + k_\phi \delta \quad (23)$$

$$= k_\phi(k_f + 2)\delta + \epsilon_2 \quad (24)$$

$$= 0 \quad (25)$$

$$\implies \phi(\mathbf{x} + \mathbf{f}(\mathbf{x}, \mathbf{u})dt) \leq \phi(\mathbf{x}) - \gamma dt \quad (26)$$

□

A.3 Safety index design and properties

It worth noting that a state satisfying $\phi < 0$ may not be safe. We denote the sublevel set of ϕ by \mathcal{X}_ϕ . \mathcal{X}_ϕ is not necessarily a subset of \mathcal{X} . But $\mathcal{X}_s := \mathcal{X}_\phi \cap \mathcal{X}$ is the forward invariant and finite time convergent safe subset [4]. To prove this, we first partition the whole state space into three parts:

- The space $\mathcal{F} := \{\mathbf{x} \mid \phi(\mathbf{x}) > 0\}$;
- The space $\mathcal{X}_s := \{\mathbf{x} \mid \phi(\mathbf{x}) \leq 0\} \cap \{\mathbf{x} \mid \phi_0(\mathbf{x}) \leq 0\}$;
- The space $\mathcal{G} := \{\mathbf{x} \mid \phi(\mathbf{x}) \leq 0\} \cap \{\mathbf{x} \mid \phi_0(\mathbf{x}) > 0\}$.

We will prove the forward invariance and finite time convergence of \mathcal{X}_s defined by the safety index we used in this work: $\phi(\mathbf{x}) = \phi_0^*(\mathbf{x}) + \alpha\dot{\phi}_0(\mathbf{x}) + \beta$.

For forward invariance, it suffices to show that all $\dot{\mathbf{x}}$ along the boundary of \mathcal{X}_s are pointing toward the interior of \mathcal{X}_s . For finite time convergence, we are going to show that under certain conditions, all trajectories starting from \mathcal{G} will converge to \mathcal{X}_s and all trajectories start in \mathcal{F} will converge to $\mathcal{X}_s \cup \mathcal{G}$.

A.3.1 Forward invariance of \mathcal{X}_s

Lemma A.1 (Forward Invariance). A piece-wise Lipschitz continuous control law that satisfies (3) will make \mathcal{X}_s forward invariant if and only if $\forall \mathbf{x}$ that satisfies $\max(\phi, \phi_0) = 0$, we have¹

$$\max\left\{\dot{\phi} \cdot \frac{0 - \phi_0}{|\phi - \phi_0|}, \frac{0 - \phi}{|\phi - \phi_0|} \cdot \dot{\phi}_0\right\} \leq 0. \quad (27)$$

Proof. Note that \mathcal{X}_s is the sub-level set of a piecewise smooth function $\phi^* := \max(\phi, \phi_0)$. We cannot directly apply Nagumo's theorem here, since it requires the scalar function ϕ^* to be smooth. Going back to the initial definition of forward invariance, which requires that the system trajectory stay within the same set. Since the closed-loop system dynamics are piece-wise Lipschitz, the system trajectory exist and is continuous. Hence \mathcal{X}_s can be forward invariant if and only if the system trajectory starting from the boundary of \mathcal{X}_s should all pointing to the interior of \mathcal{X}_s . Mathematically, that is $\forall \mathbf{x} \in \{\mathbf{x} \mid \phi^*(\mathbf{x}) = 0\}$, $\dot{\phi}^*(\mathbf{x}) \leq 0$.

$$\begin{aligned} \dot{\phi}^*(\mathbf{x}) &= \lim_{t \rightarrow 0^+} \frac{\max(\phi(\mathbf{x} + t\dot{\mathbf{x}}), \phi_0(\mathbf{x} + t\dot{\mathbf{x}})) - \max(\phi(\mathbf{x}), \phi_0(\mathbf{x}))}{t} \\ &= \lim_{t \rightarrow 0^+} \max\left(\frac{\phi(\mathbf{x})}{t} + \dot{\phi}(\mathbf{x}), \frac{\phi_0(\mathbf{x})}{t} + \dot{\phi}_0(\mathbf{x})\right) \\ &= \begin{cases} \dot{\phi}(\mathbf{x}) & \phi(\mathbf{x}) = 0, \phi_0(\mathbf{x}) < 0 \\ \dot{\phi}_0(\mathbf{x}) & \phi(\mathbf{x}) < 0, \phi_0(\mathbf{x}) = 0 \\ \max(\dot{\phi}(\mathbf{x}), \dot{\phi}_0(\mathbf{x})) & \phi(\mathbf{x}) = \phi_0(\mathbf{x}) = 0 \end{cases} \end{aligned}$$

Hence, $\dot{\phi}^*(\mathbf{x}) \leq 0$ is equivalent to the inequality (27). Note that $\frac{0-\phi_0}{|\phi-\phi_0|} = 0$ when $\phi_0 = 0$ and $\frac{0-\phi_0}{|\phi-\phi_0|} = 1$ when $\phi = 0$. Similarly, $\frac{0-\phi}{|\phi-\phi_0|} = 0$ when $\phi = 0$ and $\frac{0-\phi}{|\phi-\phi_0|} = 1$ when $\phi_0 = 0$. Hence we have verified the condition in the claim. \square

In this work, we require $(\phi(\mathbf{x} + \mathbf{f}(\mathbf{x}, \mathbf{u})dt) - \phi(\mathbf{x}))/dt < -\gamma$ or $\phi \leq 0$. Easy to verify that our requirement meet the conditions in eq. (27).

A.3.2 Finite time convergence of \mathcal{X}_s

It is obvious that all trajectories start in \mathcal{F} will converge to $\mathcal{X}_s \cup \mathcal{G}$ in finite steps because $\dot{\phi} \leq -\gamma$. ϕ will decrease to 0 in finite time. Then we consider the trajectories start in \mathcal{G} .

$$\phi = \phi_0^* + \alpha\dot{\phi}_0 + \beta \leq 0 \implies \dot{\phi}_0 \leq \frac{-\phi_0^* - \beta}{\alpha} \quad (28)$$

$\phi_0^* > 0$, $\forall \mathbf{x} \in \mathcal{G}$ because ϕ_0^* defines the same sublevel set as ϕ_0 . Therefore

$$\dot{\phi}_0 \leq \frac{-\phi_0^* - \beta}{\alpha} \leq \frac{-\beta}{\alpha}. \quad (29)$$

Then ϕ_0 decreases to 0 in finite time, therefore the trajectory will converge to \mathcal{X}_s in finite time.

A.4 Deadlock

When there are multiple obstacles, the agent needs to consider the intersection of all safety constraints, which may lead to deadlock. Safe control algorithms are generally insufficient to deal with this situation because of the lack of high level and long term information. Extending our method to multi-step MPC may address this problem.

A.5 Tracking with NNDM

We compared tracking performance of different solvers. The performance of the original Ipopt solver is too bad, so we add an extra optimality constraint to help it find a better solution. Specifically, on top of eq. (5), we add the following constraint:

$$|\mathbf{x}_{k+1} - \mathbf{x}_{k+1}^r| < \mathbf{x}_\epsilon \quad (30)$$

¹Here $\frac{0}{0}$ is defined to be 1.

where \mathbf{x}_ϵ is a constant vector we define to bound the optimized state. When the velocity term and orientation term of \mathbf{x}_ϵ are small, Ipopt is able to find a smooth trajectory as we shown in fig. 3. But if we do not emphasize the importance of velocity and orientation, Ipopt only can find jagged trajectories. fig. 5 show the trajectories and two control signals when all terms of \mathbf{x}_ϵ is 0.1.

We also show the results of the original Ipopt without any additional constraints in fig. 6.

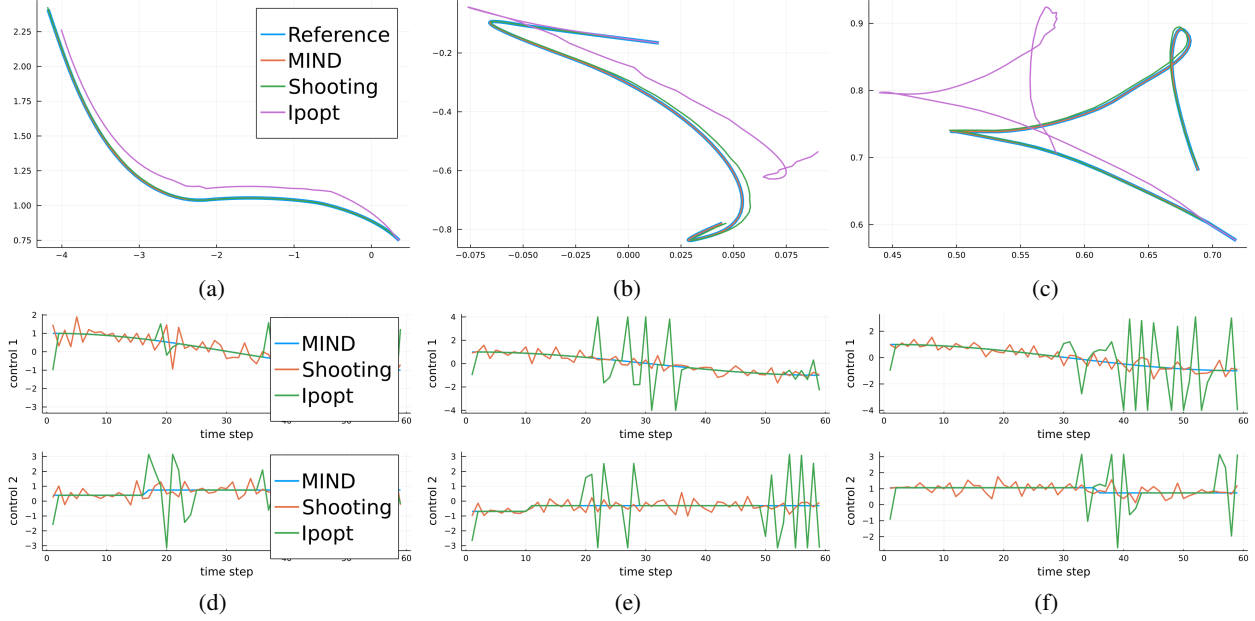


Figure 5: Trajectory tracking using MIND, shooting-100, and Ipopt. The first row shows the trajectories, and the second row shows two corresponding control signals for the trajectories.

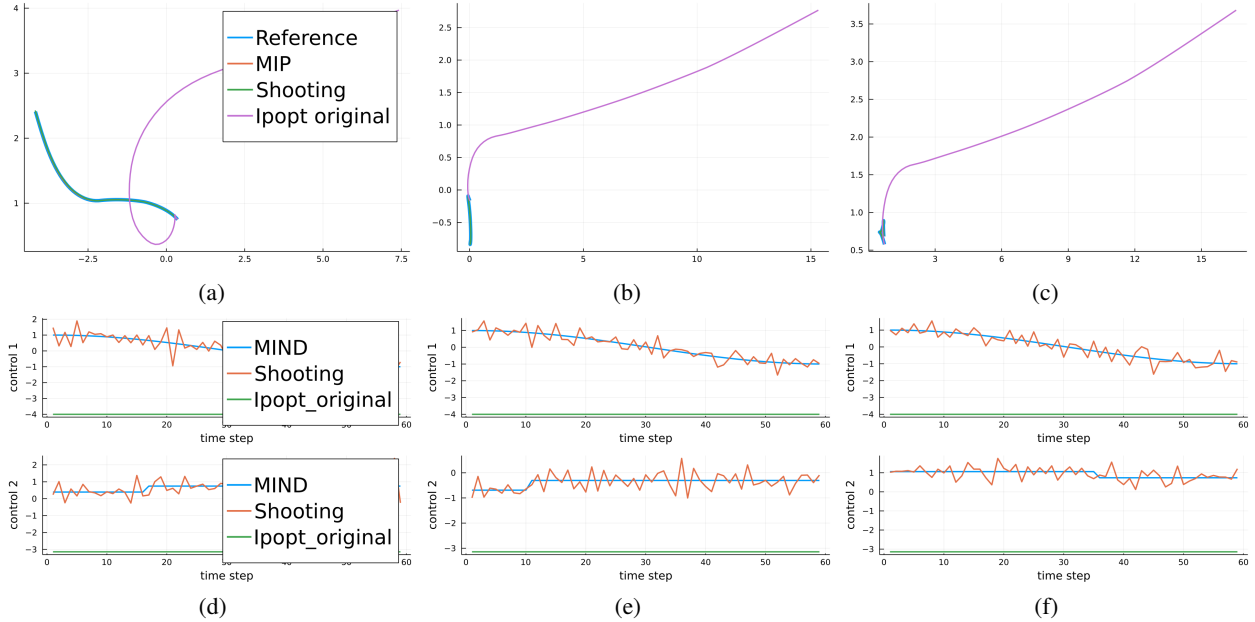


Figure 6: Trajectory tracking using MIND, shooting-100, and original Ipopt. The reference trajectories are the same as fig. 5, But the original Ipopt trajectories deviate too much. The second row shows two corresponding control signals. Original Ipopt can not find feasible control.

Hidden Dim	2-layer		3-layer		4-layer		5-layer	
	error	time	error	time	error	time	error	time
50	0.275	0.027 s	0.150	0.073 s	0.141	0.260 s	0.147	2.223 s
100	0.198	0.075 s	0.138	0.168 s	0.133	4.786 s	0.138	Stopped
200	0.188	0.141 s	0.137	7.283 s	0.134	Stopped		
300	0.190	0.231 s	0.130	Stopped				
500	0.168	0.582 s						
1000	0.163	2.327 s						

Table 3: Average norm of prediction errors after 1000 epochs training, and average computation time of MIND for one step. We early stopped the computation for some models because the time is too long for real time execution. The prediction error norm is computed by $\|\dot{\mathbf{x}} - \dot{\mathbf{x}}_{Actual}\|$. We only use this error to show their relative learning ability. A smaller error may suggest the model having a better learning ability.

A.6 MIND Scalability

We studied how MIND can scale to different model sizes. We test models with different layers and different hidden dims as shown in table 3. Besides the computation time, we also show the average prediction error of these models to demonstrate their relative learning ability. We may consider a model with a smaller error having a better learning ability. As a baseline, [7] uses a 2-layer 500 hidden dim network to learn the model of an ant robot (one torso and four 3-DoF legs), which has 111 state dimensions, with joint torque as control input. And most models (whose error is less than 0.168) we test may have better learning ability than the 2-layer 500 hidden dim one. So we may assume these models are already enough to learn a variety of complex dynamics with high dimensional input output. It shows the potential of our method to achieve real time control for models with complex dynamics.

A.7 Performance with the Actual dynamics

Although we do not consider model mismatch in this work, we test how our method can improve safety for collision avoidance tasks with the actual dynamics. We compute the safe control with the learned NNDM, and execute the control on the actual dynamics. The results are shown in table 4. Safety and efficiency (minimizing tracking error) can be conflicting objectives in some states. Therefore a ϕ^l controller may suggest control inputs that barely meet the safety constraints to maximize efficiency. And these control inputs may lead to safety violation under the actual dynamics due to model mismatch. As a future work, we will quantify the uncertainty of NNDMs, and design safety indexes that ensure safety even with uncertainty.

Metric	NNDM			Actual Dynamics		
	ϕ_0	ϕ^h	ϕ^l	ϕ_0	ϕ^h	ϕ^l
Success rate	0%	72%	100%	0%	65%	79%
ϕ_0 -violation rate	100%	0%	0%	100%	0%	21%
Infeasible rate	100%	28%	0%	100%	35%	0%

Table 4: Safety indexes under NNDM and the actual dynamics, the original safety index ϕ_0 , a synthesized safety index ϕ^h with manually tuned parameters, and a synthesized safety index ϕ^l with learned parameters on 100 randomly generated collision avoidance tasks. We consider one trial successful if there is no safety violation or infeasible state. A safe action computed with NNDM may become unsafe under the actual dynamics due to model mismatch. But ϕ^l still ensures feasibility in all cases.

A.8 Phase plots

Phase plot shows the trajectories of the system dynamics in the phase plane. We can see how different safety indexes reacts to the same situation. We draw the trajectory of $\phi = 0$ for ϕ_0 , ϕ^h , and ϕ^l , as shown in fig. 7. ϕ^l is more conservative, characterizes a smaller safe set, but ensures feasibility of all states.

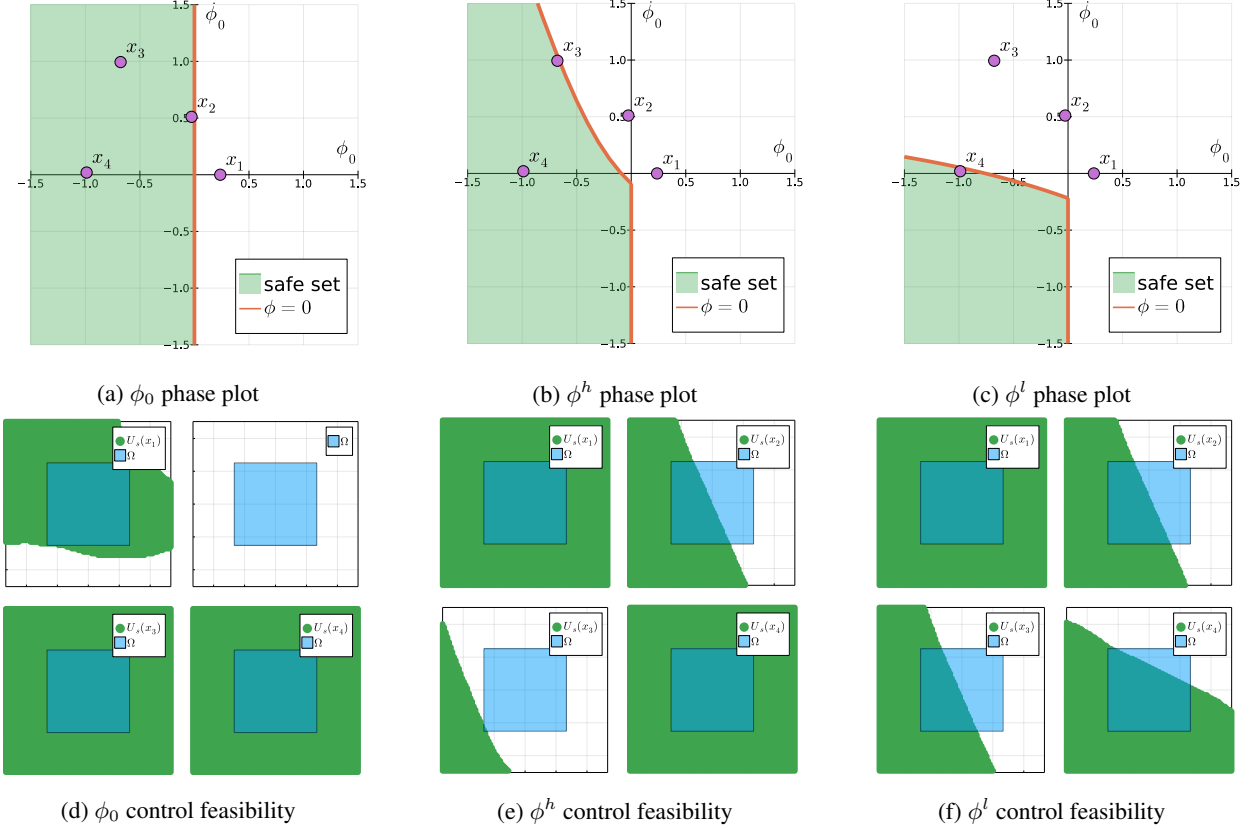


Figure 7: Phase plots and control feasibility plots. The first row shows the phase plot for different safety index. And the second row shows the control spaces at four sampled states \mathbf{x}_1 to \mathbf{x}_4 . The blue squares denotes the control limit Ω . The green areas are the feasible controls that satisfy the safety constraint. Before the safety index synthesis, there is no feasible control for \mathbf{x}_2 . And for the manually designed safety index ϕ^h , there is almost no feasible control for \mathbf{x}_3 . But for the learned safety index ϕ^l . The feasibility is guaranteed for arbitrary states.

A.9 Approximate verification methods

We use a complete method to find the optimal control, which guarantees the optimality. However, it is also possible to find an approximation to the optimal control in less time by approximate verification methods.

For example, MIP is typically solved by linear-programming based branch-and-bound algorithm [28]. The problem is constructed as a searching tree. Each leaf node corresponds to a set of values for the integer variables. The algorithm gradually narrows down the optimality gap upper bound by finding better leaf node, and disposes branches that have worse optimality gap lower bound. When all the branches are either disposed or explored, the optimal solution is found. But in fact, we can stop the optimization at any time with a best control so far, which can be used as an approximation to the optimal control.

We could also partition the control space and use reachability based methods to find an approximation of the optimal control. Given a partition of the control space, reachability methods can return a set of $\dot{\mathbf{x}}$. then an optimality gap upper bound $= \max_{\dot{\mathbf{x}}} \|\dot{\mathbf{x}} - \dot{\mathbf{x}}^r\|$. The optimality upper bound decreases with the partition goes finer, until the optimal control is found. And similar to MIP, we can drop those partitions whose optimality lower bound is higher than existing best upper bound. We can stop the process at anytime and sample a control from the partition that has the current best optimality upper bound as an approximation to the optimal control.